18th Australasian Fluid Mechanics Conference
Launceston, Australia
3-7 December 2012

Numerical simulation of the flow within a fluidic precessing jet nozzle

X. Chen, Z.F. Tian and G.J. Nathan

School of Mechanical Engineering
The University of Adelaide, SA 5005 AUSTRALIA

Abstract

This paper presents a Computational Fluid Dynamics (CFD) model of a complex, three-dimensional and oscillatory flow generated by an axisymmetric fluidic precessing jet nozzle. ANSYS has been chosen as the platform for the modelling. Compared with previous experimental results, good qualitative agreement of the main flow features and reasonable quantitative agreement of both the phase-averaged velocity contours of five planes within the nozzle and the Strouhal number that predicted by the numerical model has been achieved. The influence of cycle to cycle variation has also been discussed.

Introduction

The fluidic precessing jet (FPJ) nozzle, which is an invention of Luxton and Nathan [1], is used in rotary kilns to reduce the NO_x emissions, typically by 30-40% [2], and to increase both the output and product quality by about 5% [3]. However, at present, no reliable numerical models are available for the design and optimisation of the FPJ nozzle. The objective of the current work, therefore, is to develop a CFD model of the FPJ nozzle that achieves good qualitative agreement with the main flow features observed experimentally, reasonable agreement with the measured velocity distribution within the nozzle and the Strouhal number of precession.

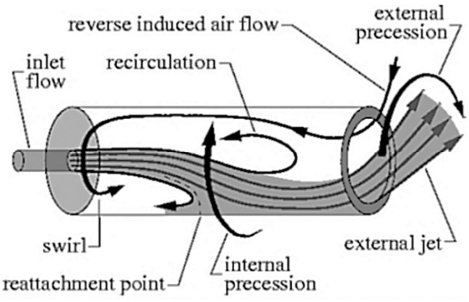

Figure 1. A schematic diagram of the fluidic precessing jet nozzle and the flow within it [4].

Figure 1 shows the components of the FPJ nozzle, which are an axisymmetric chamber followed by a large sudden expansion. The flow separates after entering the nozzle chamber through the pipe inlet and then reattaches instantaneously and asymmetrically onto the curved wall of the chamber [5]. The reattachment point moves azimuthally around the wall. Inside the chamber is a region of reverse flow, which finishes in a region of swirling fluid at the back of the chamber [6]. The emerging jet flow occupies about one third of the outlet plane when leaving the nozzle [7]. It emerges with a non-circular cross-section [8] and a deflection angle of typically 30° to 60° relative to the nozzle axis due to the pressure gradient, which is increased by the presence of the small lip at the end of the nozzle [6]. To increase the probability of jet precession above that which occurs in the configuration of Figure 1, a centrebody (CB) can be added into the chamber, slightly upstream from its outlet as shown in figure 2 [6]. These large scale features are chosen as the qualitative features with which to assess the performance of the model.

The velocity field within the FPJ nozzle has been investigated with Laser-Doppler anemometry (LDA) by Wong [9]. Phase averaged velocity contours at different transverse planes in the nozzle were measured to provide information of the instantaneous structure of the flow [10]. Also, It has been found previously from various velocity measurements that the flow varies greatly from cycle to cycle [10]. However, the significance of this variation is still unclear to date.

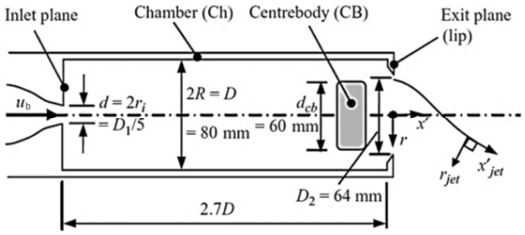

Figure 2. Precessing jet nozzle with centrebody [10].

Xu et al. [11] have numerically investigated on the velocity field of precessing jet generated by triangular oscillating jet nozzle by Large Eddy Simulation (LES). Guo et al. [12] have adopted Very Large Eddy Simulation (VLES) to simulate flow generated by a nozzle with sudden-expansion that similar to the FPJ nozzle, but with much larger length to diameter ratio. The predicted Strouhal number has been compared with experimental result and good quantitative agreement has been achieved in both of the above researches. However, the phase-averaged velocity validation in the above researches is limited, and there is no CFD study on the flow produced by FPJ nozzle.

The current work aims to verify that the resolution of the large eddy containing oscillation can result in reasonable accuracy of the calculated flow-field. Besides, to understand how does the large cycle to cycle variations been produced and its effect on the phase-averaged flow within the chamber is also purposed in this research.

Numerical approach

The geometrical configuration chosen for the work was identical to Wong's experimental configuration [9],which is shown in figure 2. It was drawn by using "Pro Engineer" and ANSYS. Figure 3 shows both the full view of the whole structure and the detailed view of the nozzle chamber with the centre-body and lip. According to Morel's [13] suggestion, the contraction was designed following a 5th order polynomial profile (equation 1) and the contraction area ratio is 10.03. The diameter of the big domain downstream from the nozzle exit plane, which is shown in the upper part of figure 3, is $12.9D_1$, and its total length is 4240mm.

$$y = H_i + (H_i + H_o)[-10\xi^3 + 15\xi^4 - 6\xi^5] \qquad (1)$$

Here, $\xi = \frac{x}{Length\ of\ the\ contraction}$.

Nomenclature	
u_i	bulk inlet velocity
ri	nozzle's inlet radius
r	distance between the point and the geometry centreline
d	nozzle's inlet diameter
R	nozzle radius
R_2	nozzle's outlet radius
D	nozzle diameter
D_{cb}	diameter of centre body
D_2	diameter of the nozzle's exit
H_i	radius of flow conditioner's inlet
H_o	radius of flow conditioner's outlet
x	axial distance along geometric centreline from the nozzle's inlet
x'	axial distance along geometric centreline form the nozzle's outlet
f_p	mean precession frequency
A	ratio of the length scale to d
B	ratio of the characteristic velocity to u_b
ϑ	angle between jet centreline and nozzle centreline

The mesh in the current research was generated by "ICEM". "O-grids" was adopted to ensure a good mesh quality near to the boundary of the nozzle. The total number of cells is 1.2 million, while it is approximately 0.3 million within the FPJ chamber. The number of cells across the diameter of the inlet to the nozzle chamber, across the diameter of the chamber and along the length is 50, 136 and 110 respectively. The mesh is finer near to the inlet of the nozzle, and the mesh close to the chamber's wall is the finest, where the nodes interval is five times closer than the most area within the chamber.

The velocity of the inlet in the model, which is the inlet of the flow conditioner, was set as 7.81m/s to ensure that the velocity at the inlet of the nozzle chamber is identical to Wong's [9] experiment, which is 78.7m/s.

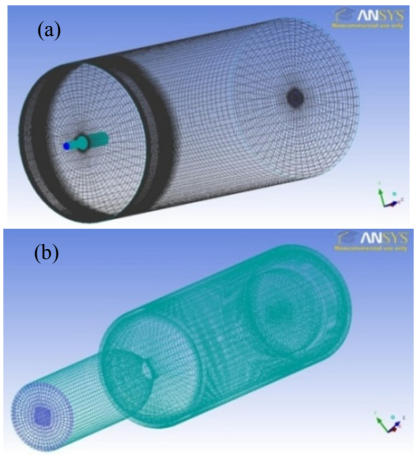

Figure 3. Geometry and mesh of the current model. (a) The whole domain, (b) Detailed view of the PJ nozzle.

In any turbulence modelling, care must be taken in the choice of the grid resolution and, for an unsteady model, of the temporal resolution. Only direct numerical simulation is sufficiently detailed to resolve all the spatial and temporal scales of turbulence, while large eddy simulation resolves the larger-scales turbulence and models the sub-grid-scales of turbulence. While Reynolds averaged Navier-Stokes (RANS) models are typically used to resolve only the average flow-field, here we take the approach of seeking to resolve the phase-averaged flow field using an unsteady RANS model (k-ε). To achieve this, it is necessary for the simulation to resolve the large-scale oscillations (i.e. the precession) within the chamber.

A "monitor point" was chosen to exactly match the equivalent point chosen by Wong for the experimental investigation, to assess by an Eularian record of velocity, the time-varying oscillations o the precession cycle. It was located 300mm from the wall of the chamber in the transverse plane which is in the half-way between the centrebody and the lip. The method chosen to calculate the phase averaged velocity was also chosen to exactly match the experimental approach of Wong [9] to allow a direct comparison. The period of each cycle was divided into 36 bins, each of ten-degrees.

The precession frequency in Wong's [9] experiment is around 7.5HZ, which corresponds to a period of 0.13 seconds. In order to ensure that the data is enough in each ten-degree range, time step in the current model is set as 0.0001 second. The data will be recorded every five time steps. Hence, the estimated number of data that can be recorded in each ten-degree range in each cycle is about 7. The results in this paper were calculated using data from the simulation time second 8.5 to second 11.

Result and discussion

Flow features

The trajectory of the precessing jet flow obtained by experiment and simulation model are shown in figure 4 and 5 respectively. Note that the trajectory in figure 4 was extrapolated from the axial velocity experimental data. Compared with both figures 1 and 4, the simulation result presents good qualitative agreement of the all the four key flow features with the experiment. The jet was calculated to reattach asymmetrically to the internal of the chamber wall as per the experiment. The reverse flow on the opposite side of the chamber was also calculated to occur, driving a swirling flow at the inlet to the chamber. The emerging jet is also deflected across the nozzle axis at a large angle of approaching 60 degrees, again qualitatively similar to experiments. A smaller reverse flow is also found underneath the reattaching jet, again consistent with experiments. The ratio of reattachment length to the inlet diameter is 5.3 in the experiment, while it is approximately 5.9 in the numerical result, which is about 10 percent longer [9].

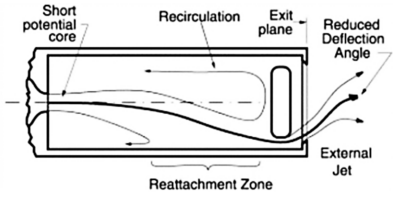

Figure 4. Transverse view of the flow measured by LDA data [9].

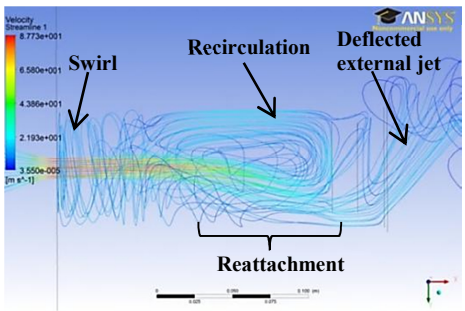

Figure 5. Streamlines of the precessing jet flow predicted by the unsteady k-ε simulation.

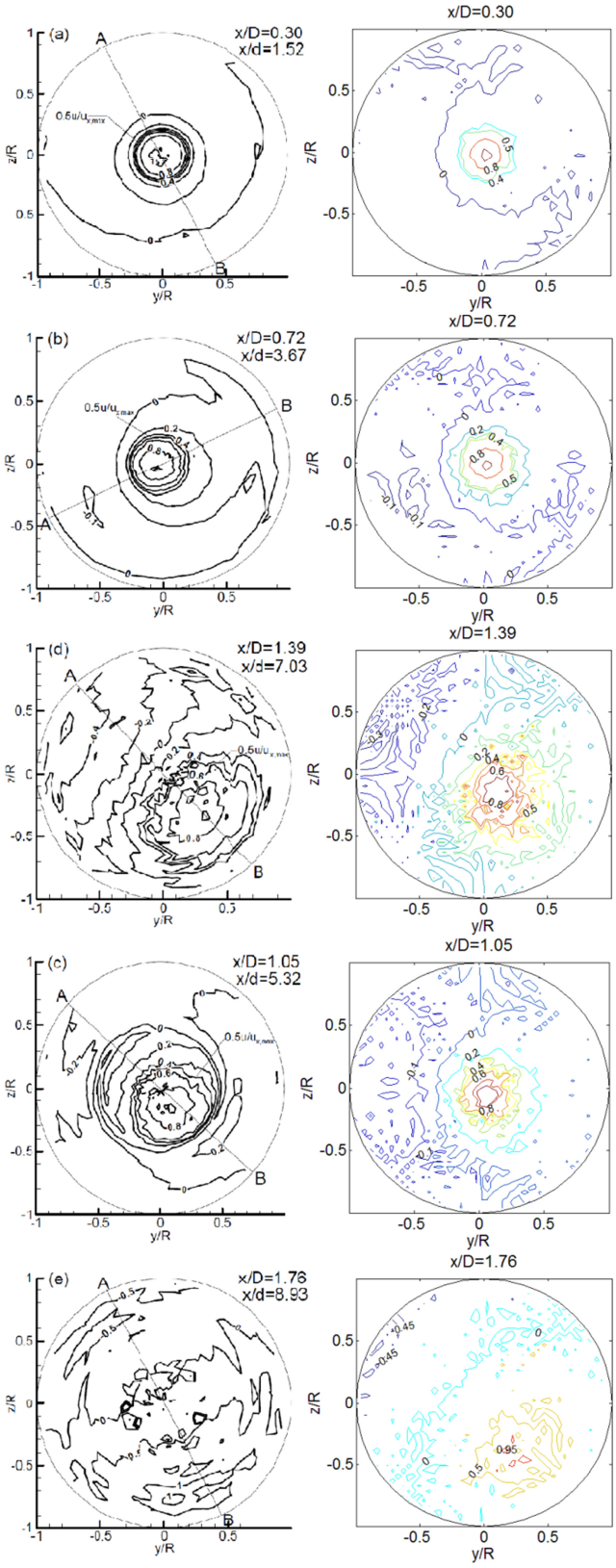

Figure 6. Comparison of phase-averaged axial velocities contours in the FPJ nozzle obtained by experiment (left) and simulation (right). Data are normalized with the local centreline velocity in each plane [9].

Internal velocity field

Five phase-averaged axial velocity contours calculated by the *k-ε* model in the FPJ nozzle are presented in figure 6 in comparison with the experimental data. The velocity data are normalised by the maximum velocity in each plane. In Wong's study [9], the area enclosed by the half-maximum velocity contour is taken as a measure of the cross section of the jet. The location of the jet and the reverse flow in the model is consistent with experiment data. As with the experiment, the diameter of the local jet increases as it traverses through the chamber. The normalized velocity values of the predictions are in close agreement with the measured values.

Figure 6 shows that the predicted jet area is smaller than the measured area. Close inspection of the case x/D = 1.76 reveals that the model slightly under-predicts the reattachment length, since the real jet is fully attached to the wall, as indicated by a cresent-shaped cross section, while the model predicts a circular cross section that is just beginning to interact with the wall. This, in turn, suggests that the model slightly under-predicts the rate of spreading of the local jet within the chamber. Future work will assess this in more detail.

Strouhal number

The Strouhal number (St) is a dimensionless parameter that is widely used to characterise oscillatory flows. Equation 2 shows the definition of the Strouhal number developed by Wong [9], which is adopted here.

$$S_t = \frac{f_p A d}{B u_b} \sin\theta \qquad (2)$$

Following previous experimental approaches, the frequency of precession was analysed from a time-record of the velocity field at a representative point in the flow. The "monitor point 2" chosen for this assessment matches exactly the measurement point chosen in the experiment, i.e., r/R_2=1.16 and x'/D_2=0.15. The spectrum, shown in figure 7, is obtained by a fast Fourier transform (FFT) from the simulation result. The frequency corresponding to the peak of the spectrum is defined as the precession frequency, which is 8.98Hz in this simulation. It is approximately 16.5% higher than the measured frequency of 7.5Hz.

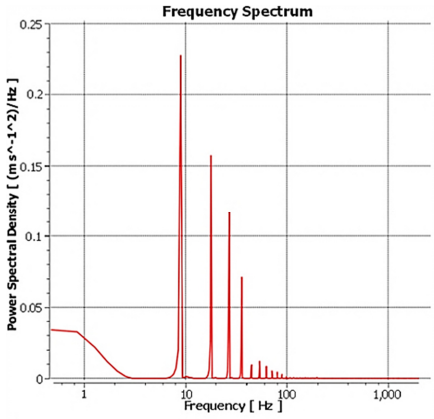

Figure 7. Frequency spectrum of the FPJ flow predicted by simulation.

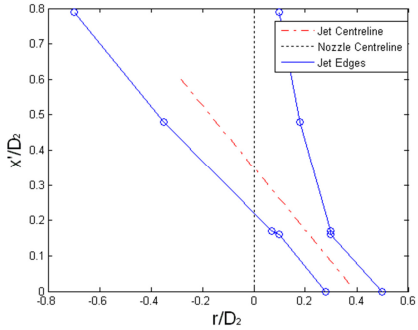

Figure 8. Predicted trajectory of the jet emerging from the nozzle's exit based on the phase-averaged velocity result.

The area within the half-maximum velocity contour of the transverse plane is taken as a representative measure of the jet area. The length scale in the current research adopts the round jet diameter based on equivalent area of the jet, and the characteristic velocity is the bulk axial velocity of the jet. The jet centreline is drawn based on the edge of the jet, shown in figure 8, to achieve the angle between jet centreline and nozzle centreline, θ.

All the related parameters for the Strouhal number calculation of both the experiment and simulation result are presented in table 1. It shows that the Strouhal number predicted by the current simulation is 17% less than the experiment result.

	f_p (Hz)	A	d (mm)	B	u_b (m/s)	θ (°)	S_t
Experiment	7.5	2.47	15.79	0.18	78.7	37	0.0124
Simulation	8.98	1.2	15.79	0.099	78.7	28	0.0103

Table 1. Strouhal number comparison.

Cycle to cycle variation

Figure 9 presents the experimentally derived frequency spectrum of the FPJ flow [9]. The predicted spectrum has a very narrow frequency peak, which shows that the precession is almost perfectly regular, while the real spectrum is much broader, consistent with the large cycle-to-cycle variation.

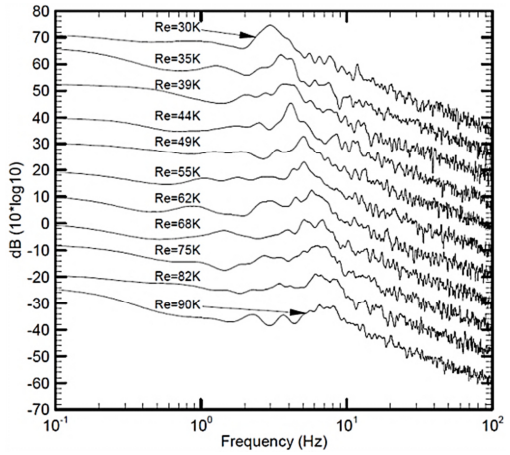

Figure 9. Experimentally derived frequency spectrum for Red=30,000 to 90,000. Vertical scale is the arbitrary spectrum in dB(10*log10) for Red=90K. The ordinate origins of the spectra for the rest Reynolds numbers are shifted upwards by +10dB [9].

Figure 10 presents the time-history of the calculated axial velocity of the flow at the monitor point 1, which is used to determine the start and end time in each cycle, in one second. It also shows that the cycles are exactly repeatable from one cycle to the next. This is in clear contrast to the experiment.

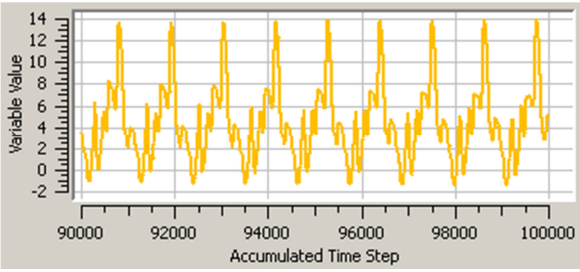

Figure 10. Axial velocity variation of the monitor point from time step 90000 to 100000 (1 second).

Conclusions

The comparison between the predicted and measured result show that the chosen spatial and temporal resolution is sufficient to achieve good qualitative agreement and reasonable quantitative agreement with the phase-averaged flow within the chamber. Better quantitative agreement can be expected by adjustment of the constants in the *k-ε* model.

This level of grid resolution results in the calculated oscillation being perfectly regular from one cycle to the next. This implies that the large cycle-to-cycle variability that occurs in practice is due to the amplification of smaller-scales of turbulence within the local jet by the flow within the chamber. Although the current spatial and temporal resolution is sufficient to resolve the large-scale oscillation, it is insufficient to resolve the large eddies within the local jet.

The above results also show that it is not necessary to resolve the cycle-to-cycle variations in order to achieve good modelling of the phase-averaged flow within the chamber. However, it is necessary to note that the flow outside the chamber is yet to be assessed, so it is premature to draw any conclusions about the accuracy of the model with regard to mixing or reacting flows.

References

[1] Nathan, G. and R. Luxton, *CONTROLLING THE MOTION OF A FLUID JET*, 1988, WO Patent WO/1988/008,104.

[2] Manias, C. and G. Nathan, *Low NOx clinker production[at Swan Portland Cement Ltd., Rivervale, Perth, W. Australia]*. World cement, 1994. **25**(5): p. 54-6.

[3] Nathan, G. and C. Manias, *The role of process and flame interaction in reducing NOx emissions.* Combustion and Emission Control, 1995: p. 309-318.

[4] Wong, C., G.J. Nathan, and T. O'Doherty, *The effect of initial conditions on the exit flow from a fluidic precessing jet nozzle.* Experiments in Fluids, 2004. **36**(1): p. 70-81.

[5] Nathan, G.J., *The enhanced mixing burner*, in *Mechanical Engineering*1988, University of Adelaide: Adelaide.

[6] Nathan, G., S. Hill, and R. Luxton, *An axisymmetric 'fluidic' nozzle to generate jet precession.* Journal of Fluid Mechanics, 1998. **370**(1): p. 347-380.

[7] Wong, C.Y., et al., *Phase-averaged velocity in a fluidic precessing jet nozzle and in its near external field.* Experimental Thermal and Fluid Science, 2003. **27**(5): p. 515-524.

[8] Nathan, G.J., et al., *Impacts of a jet's exit flow pattern on mixing and combustion performance.* Progress in Energy and Combustion Science, 2006. **32**(5-6): p. 496-538.

[9] Wong, C.Y., *The flow within and in the near external field of a fluidic precessing jet nozzle*, 2004, The University of Adelaide.

[10] Wong, C.Y., G.J. Nathan, and R.M. Kelso, *The naturally oscillating flow emerging from a fluidic precessing jet nozzle.* Journal of Fluid Mechanics, 2008. **606**(1): p. 153-188.

[11] Xu, M., J. Mi, and P. Li, *Large Eddy Simulation of an Initially-Confined Triangular Oscillating Jet.* Flow, Turbulence and Combustion, 2011: p. 1-20.

[12] Guo, B., T.A.G. Langrish, and D.F. Fletcher, *Numerical simulation of unsteady turbulent flow in axisymmetric sudden expansions.* Journal of fluids engineering, 2001. **123**: p. 574.

[13] Morel, T., *Comprehensive design of axisymmetric wind tunnel contractions.* Journal of fluids engineering, 1975. **97**(2): p. 225-233.